Nuclear Instruments and Methods in Physics Research A 609 (2009) 114–121

Contents lists available at ScienceDirect

Nuclear Instruments and Methods in Physics Research A

journal homepage: www.elsevier.com/locate/nima

First measurements of the performance of the Barrel RPC system in CMS

A. Colaleo [a,*], F. Loddo [a], M. Maggi [a,*], A. Ranieri [a], M. Abbrescia [b], G. Iaselli [b], B. Marangelli [b], S. Natali [b], S. Nuzzo [b], G. Pugliese [b,*], F. Romano [b], G. Roselli [b], R. Trentadue [b], S. Tupputi [b], P. Baesso [c], A. Grelli [c], M. Necchi [c], D. Pagano [c], S.P. Ratti [c], P. Vitulo [c], C. Viviani [c], P. Paolucci [d], D. Piccolo [d], A. Cimmino [e], D. Lomidze [e], P. Noli [e], L. Benussi [f], M. Bertani [f], S. Bianco [f], D. Colonna [f,i,p], F.L. Fabbri [f], A. Dimitrov [g], L. Litov [g], B. Pavlov [g], P. Petkov [g], T. Anguelov [h], V. Genchev [h], P. Iaydjiev [h], B. Panev [h], S. Stoykova [h], G. Sultanov [h], R. Trayanov [h], T. Christiansen [i], R. Guida [i], I. Segoni [i], C.A. Carrillo Montoya [j], G. Polese [k], A. Korpela [k], T. Tuuva [k], K. Bunkowski [l], M. Cwiok [l], K. Doroba [l], A. Kalinowski [l], M. Konecki [l], J. Krolikowski [l], K. Kierzkowski [l], I.M. Kudla [l], W. Oklinski [l], M. Pietrusinski [l], M. Bluj [m], T. Fruboes [m], M. Gorski [m], R. Gokieli [m], M. Kazana [m], M. Szleper [m], G. Wrochna [m], P. Zalewski [m], K.T. Pozniak [n], W. Zabolotny [n], William Whitaker [o]

[a] INFN Sezione di Bari, Italy
[b] Dipartimento Interateneo di Fisica and Sezione INFN, Bari, Italy
[c] Dipartimento di Fisica Nucleare e Teorica and Sezione INFN, Pavia, Italy
[d] INFN, Sezione di Napoli, Italy
[e] Dipartimento di Fisica e Sezione INFN, Napoli, Italy
[f] INFN Laboratori Nazionali di Frascati, Italy
[g] Faculty of Physics, Sofia University, Bulgaria
[h] INRNE, Bulgarian Academy of Sciences, Bulgaria
[i] CERN, Geneva, Switzerland
[j] Universidad de Los Andes, Bogota, Colombia
[k] Lappeenranta University of Technology, Finland
[l] Institute of Experimental Physics, University of Warsaw, Warsaw, Poland
[m] Soltan Institute for Nuclear Studies, Warsaw, Poland
[n] Institute of Electronics Systems, Warsaw University of Technology, Warsaw, Poland
[o] California State University, Fresno, USA
[p] Facoltá Ingegneria Universitá di Roma "La Sapienza", Italy

ARTICLE INFO

Article history:
Received 25 February 2009
Received in revised form
18 June 2009
Accepted 20 July 2009
Available online 14 August 2009

Keywords:
CMS
RPC
MTCC
Resistive Plate Chamber

ABSTRACT

During the summer 2006, a first integrated test of a part of the CMS experiment was performed at CERN collecting a data sample of several millions of cosmic rays events. A fraction of the Resistive Plate Chambers system was successfully operated. Results on the RPC performance are reported.

1. Introduction

The Compact Muon Solenoid (CMS) [1,2] experiment at the Large Hadron Collider (LHC) is based on high magnetic field (4 T), which, with the fine read-out granularity of the detector trigger system, will allow a preliminary transverse momentum assignment of muons [3]. The bunch crossing (BX) period of the proton beams has been designed to be 25 ns to achieve high luminosity. A high time resolution trigger detector is, therefore, required to properly determine the BX assignment of the muon candidates. CMS is equipped with a redundant Muon system based on Drift Tube (DT) chambers and Cathode Strip Chambers (CSC), respectively in the barrel and endcap regions, for precise position

* Corresponding authors.
E-mail addresses: Marcello.Maggi@ba.infn.it (M. Maggi), Gabriella.Pugliese@ba.infn.it (G. Pugliese).

0168-9002/$ - see front matter © 2009 Published by Elsevier B.V.
doi:10.1016/j.nima.2009.07.099

measurement. In addition, Resistive Plate Chambers (RPC) are used for bunch crossing identification. The RPC trigger system is one of the largest ever built detector employing this technology [2].

In summer 2006, for the first time, the CMS detector was closed and the super-conducting magnet was ramped up to its nominal value for commissioning and field map measurements. During this test, named Magnet Test and Cosmic Challenge (MTCC) [4], a portion of the Muon and the calorimeter systems was operated under cosmic rays to study the global CMS behavior by combining information from different sub-detectors. Advanced versions of the final read-out, data acquisition and control system protocols were employed. The main goals for the RPC system were the determination of the synchronization and operation procedures, the assessment of the trigger capability and the study of the chambers' performance.

This paper only reports results on the performance of the RPC barrel system. For further information on the MTCC, the reader is referred to Ref. [4].

2. Experimental set-up

In the barrel iron yoke, the RPC muon chambers form six coaxial sensitive cylinders around the beam axis approximated with concentric dodecagon arrays and subdivided into five wheels composed of 12 sectors. The sectors of each wheel cover a region of 30° in ϕ and about 0.1 in pseudorapidity η with projective read-out geometry with respect to the interaction point. The wheels are denoted, hereafter, by the notation W_i where i is in the $-2, 2$ range and the relative sector number runs from 1 to 12. Each sector of a wheel comprises six layers of RPC chambers. Two layers are in the first and second Muon station above (Inner) and below (Outer) the DT chamber. The third and fourth Muon stations are equipped only with the Inner layer that is covered by two RPC muon chambers apart from few sectors. In sectors 4 and 10 the fourth station comprises two DT chambers, each with one (sector 4) or two (sector 10) RPC chambers. In sectors 9 and 11 there is only one RPC muon chamber in the fourth station. A more detailed geometrical description of the detector can be found in Ref. [5].

Each chamber is read-out by electrode strips running along the beam-axis direction to measure the transverse momentum of the muon particles. The strip width varies from 2.3 cm for the inner layer to 4.1 cm for the outer layer. To improve the time resolution, the strips are divided into two or three parts called η-partitions. During the MTCC, three bottom sectors, sectors 10 and 11 belonging to W_{+2} and sector 10 of W_{+1}, were operated. Fig. 1 shows a (r, ϕ) schematic view of wheel W_{+2} with the sectors under test highlighted.

The 23 chambers, representing 5% of the entire Barrel RPC system, were all operated at a nominal voltage of 9.2 kV. The chambers reached, in this conditions, 90% efficiency or higher. Most of the results are given in terms of the effective operating voltage, HV_{eff}, which is obtained from the nominal values after pressure and temperature corrections, to account for their variations during the running period [6]. On average HV_{eff} was about 9.6 kV. The CMS RPC standard gas mixture, i.e. 96.2% $C_2H_2F_4$, 3.5% i-C_4H_{10}, 0.3% SF_6, was used.

The strip signals were discriminated and shaped into 100 ns logic pulses by the front-end boards [7] with 220 mV threshold, corresponding to a minimum signal charge of about 120 fC to be compared with an average minimum ionizing particle signal of about 1 pC. All signals are propagated to the Link Boards (LB) placed on the detector periphery. The LBs synchronize the signals to the 40 MHz clock and, after data compression, send them to the Trigger Boards located in the control room, where the trigger algorithm based on pattern recognition is performed by Pattern

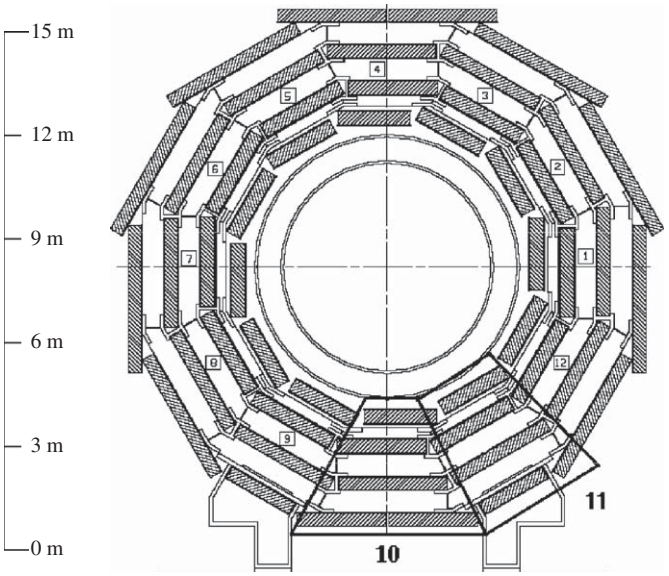

Fig. 1. An (r, ϕ) schematic view of a 15-m height CMS wheel W_{+2}. The sectors 10 and 11, under test, are highlighted.

Comparator (PAC) devices [8]. The Trigger Boards are part of the readout chain and data were also collected via their control system that allows an event-dump mechanism.

The PAC algorithm has been specifically developed to identify muon tracks coming from the interaction point. It is, therefore, not optimized for atmospheric muons, although some provisional modification of the algorithm for the sectors under operation made possible its application for the MTCC and limited used for debugging purpose. In addition, in view of detector commissioning and maintenance during the LHC shutdown periods, the development of a special RPC trigger for cosmic ray muons has been foreseen: the RPC Balcony Collector (RBC) that was implemented in the system and used as a main trigger signal. The RBC receives from the LB the logical OR signal of each η-partition. The trigger logic is based on a Pattern Comparator with a preloaded pattern set and produces a sector-based cosmic trigger with a selectable majority level from 1/6 to 6/6. It has, in addition, several features such as masking and forcing capability of the η-partitions to increase the trigger selectivity on specific patterns and extra latency configuration for synchronization purposes. More details on the RBC trigger electronics can be found in Ref. [9]. During the MTCC, the DT system was also providing trigger. This was exploited in this analysis for an unbiased study of the RPC system.

A sample of about 20 million events was collected with both RBC and DT triggers used singly or in logical combination depending on the quality of the trigger.

3. Experimental methods

The interplay between the RPC and DT system allows the determination of the timing of the trigger system and establish local reconstruction for fast determination of the RPC performance.

At the LHC the crossings of beam bunches occur every 25 ns. The muons which originate from the proton–proton collisions are produced with very narrow timing (the RMS bunch length during collisions is estimated to be 7.55 cm and so the bunches overlap time duration is about 1 ns). However, the chamber hits are spread in time as the result of several effects like the difference of muon

track lengths with different bending and the signal propagation along the strips [10]. Moreover, the total timing of the signals received by the LBs varies among them, since the chambers have different distances to the interaction point and the cables connecting the chambers with the LBs also have different lengths. The asynchronous signals from chambers are assigned to the proper clock period by the Synchronization Unit of the LBs.

A time window is set such that all muon hits, originating from the same bunch crossing, are assigned to the proper clock period [11]. An initial window position is calculated on the basis of the muons' time-of-flight and the length of the signal cables. A subsequent analysis of the initial collected data allows the refinement of the time window position. In case of the cosmic muons (distributed randomly in time) the position of the windows can be defined with arbitrary offset (the same for all LBs). The distributions of the chamber hits BX with respect to the trigger time are presented in Fig. 2. BX number equal to 1 corresponds to the trigger signal. By changing the global offset, the RPC trigger can also be aligned with the trigger signals provided by the Drift Tube system. The difference between the two reception times, before and after the correction, is shown, respectively, in Fig. 3a and b. Only the events where both systems produced the trigger are included. The symmetry in the resulting distribution demonstrated the optimal timing behavior reached.

In the first three stations, the DT local reconstruction allows the determination of segments in the 3D space obtained by analyzing hits in each of the three super-layers, comprised in the DT chambers [2]. Unbiased predictions of the hit positions of cosmic muons on the RPC system are obtained by extrapolating linearly the DT track segments to the nearest RPC chambers. This information is used to determine the detailed local performance of the chambers. The residuals of the reconstructed hit position in the RPC to the track segment extrapolated point are shown in Fig. 4. The width of the residuals is $\sigma = 1.02$ cm, compatible with the expected space resolution of 1.01 cm.

Both the synchronization and the local reconstruction show the excellent correlation of the responses of the two muon systems.

4. Noise studies

The use of RPC as trigger detector requires a low noise level to allow the proper functioning of the algorithm and to limit the number of fake triggers. Noise hits can cause fake triggers by promoting low transverse momentum muons to higher momenta [12]. The measurement of the performance of the chambers is also affected by the noise. It is, therefore, crucial to determine the noise of the detectors in working running conditions.

Noise rates have been measured under different conditions and during dedicated short periods by an online procedure before each data taking, and by dedicated offline data analysis method. In the online procedure, strips with a rate larger than 10 Hz/cm^2 are masked during the data taking and are, therefore, excluded in the results presented here.

4.1. Online analysis

The noise rates are evaluated from calibration procedures taken at the beginning of each data-taking period. The strip signals were counted by the dedicated multi-channel counter modules implemented in the LBs [10].

Noise profiles and history summary plots for each chamber were continuously produced during the entire period of data taking. The number of dead channels was 0.2% and the number of strips exceeding the noise rate of 10 Hz/cm^2 was 1.2%. Most of the masked strips were due to faulty front-end boards which required maintenance. In Fig. 5 the overall noise distribution for all the chambers under test is plotted for different values of the magnetic field. No significant dependence on the magnetic field was observed.

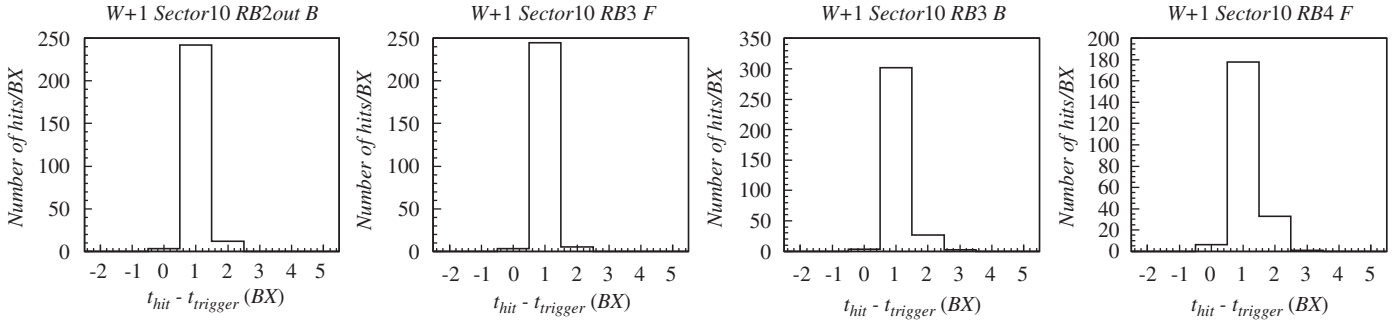

Fig. 2. Distributions of the chamber hit timing with respect to the trigger time. BX number equal to 1 corresponds to the trigger signal. BX corresponds to 25 ns.

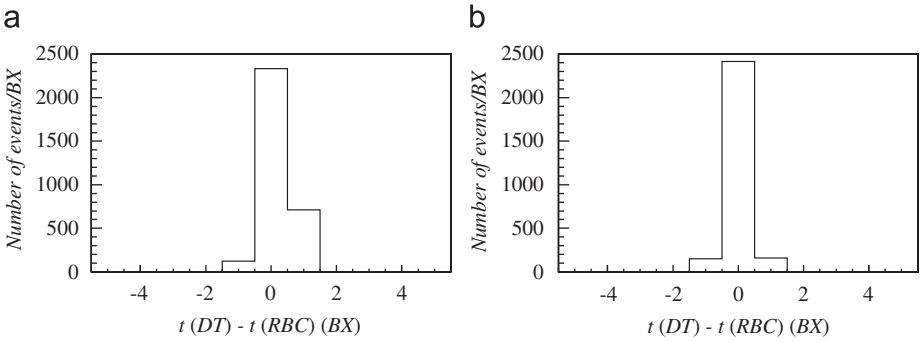

Fig. 3. Trigger reception time difference between DT and RBC signals before (a) and after (b) global timing offset corrections.

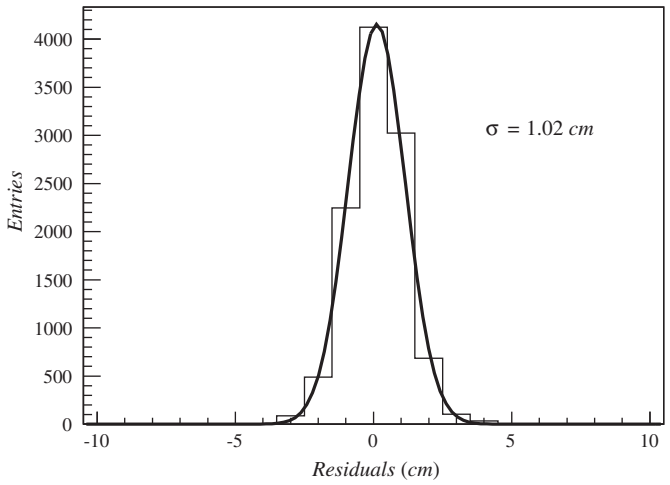

Fig. 4. Distribution of residuals between the extrapolated track impact point, as determined by the DT segments, and the center of RPC cluster on one representative chamber.

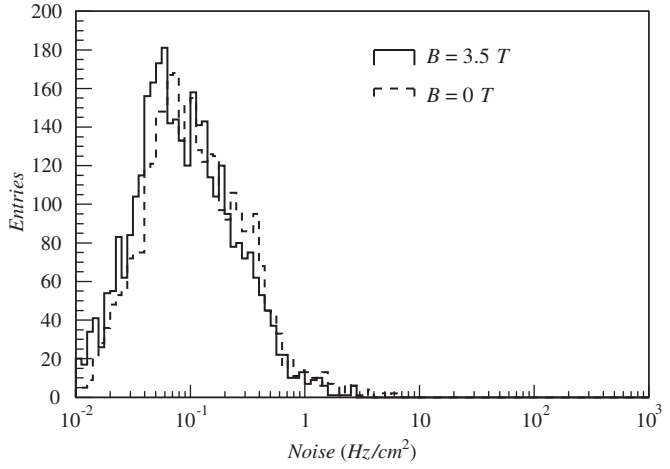

Fig. 5. Overall noise distributions of the RPC system for two magnetic field values. All chambers under test are considered.

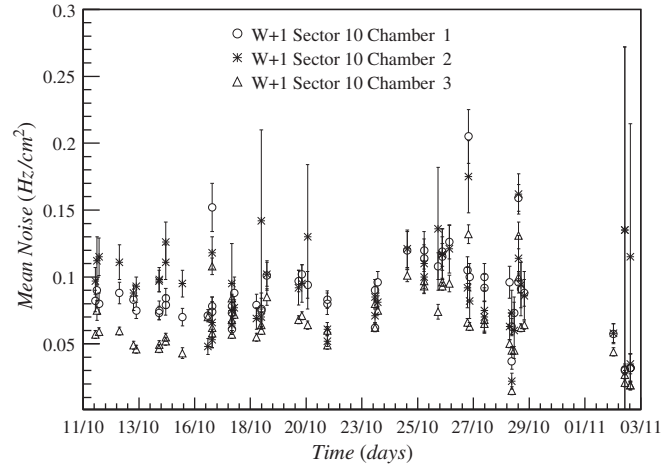

Fig. 6. Average noise time chart for few chambers. The data were collected during the entire data taking period before each run.

Fig. 6 shows a history plot of the average noise over the entire data taking period for some representative chambers. The system was stable in all the configurations it was operated. The

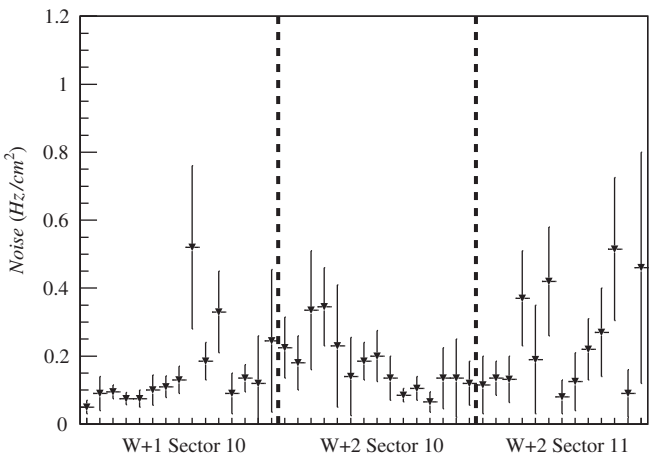

Fig. 7. Profile histogram of the noise distribution for the system in operation. Each bin of the distribution corresponds to an η-partition. The average, represented by the full triangle, and the spread, represented by the bars, are calculated from all the measurements performed.

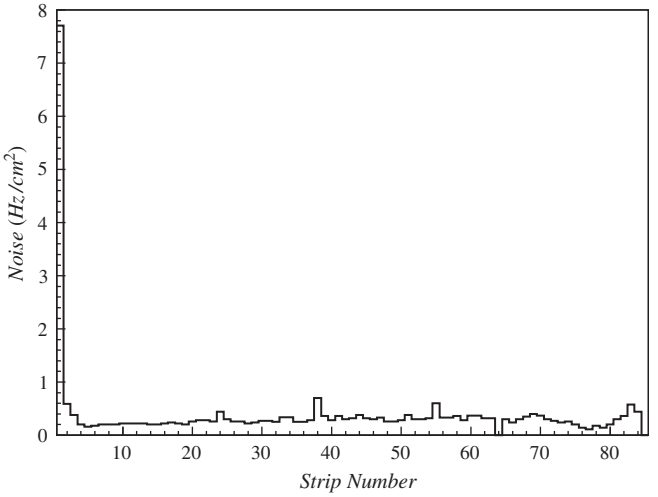

Fig. 8. Average noise strip profile for one η-partition with relatively large average noise. The large average value is determined by the first strip.

measurement of average noise for the entire system under test is shown in Fig. 7, where, for each η-partition, the rate was determined over the entire running period. The spreads of all measurements are represented by the bars. The detailed strip profile of one particular η-partition affected by relatively large noise is presented in Fig. 8. In this case the higher rate is due to a single strip just below the masking threshold.

4.2. Offline noise analysis

An independent evaluation of the noise rate was performed by selecting events triggered by the DT system. In each event only sectors for which, no DT segments are found and to which the DT segments of the other sector do not extrapolate to any RPC chamber, are considered. This procedure is designed to select regions far from the real muon track. A visual scan of several events is also performed to check the reliability of the method. The noise rate is determined by the number of observed reconstructed hits divided by the total acquisition time that is given by the number of events and the number of BX read-out. A typical noisy strip multiplicity distribution is given in Fig. 9 that

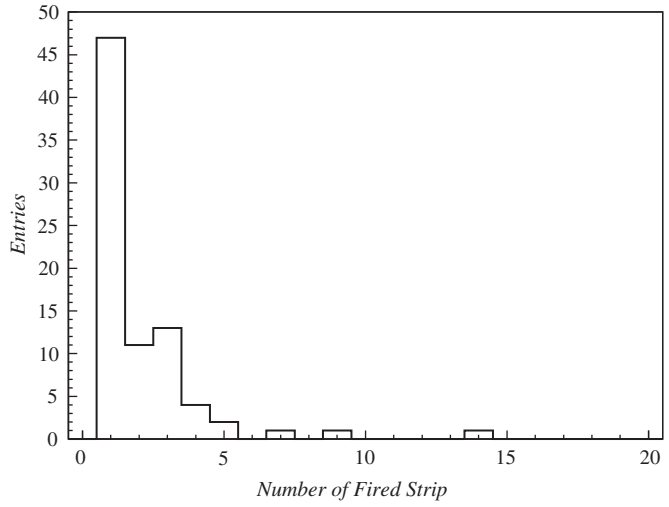

Fig. 9. Noisy strip multiplicity distribution for sector 10 of W_{+1}.

Table 1
Average noise values of all three sectors under test as obtained by the offline analysis.

	Noise (Hz/cm^2)
W_{+2} sect. 10	0.11 ± 0.02
W_{+2} sect. 11	0.44 ± 0.06
W_{+1} sect. 10	0.34 ± 0.05

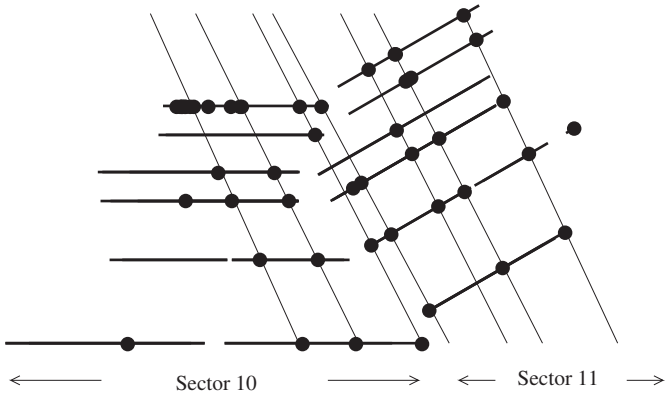

Fig. 10. Event display of a multi-muon cosmic event. Superimposed the result of a RPC stand-alone reconstruction.

shows the result obtained for sector 10 of W_{+1}. No events were found with a strip multiplicity exceeding 20 strips fired.

While the online method is sensitive to noise appearing at the beginning of each run for a very short period, the offline method measures the average noise during the data taking runs and so it includes also to eventual sporadic hot channels that appear within a run. Using this method, the average noise values of the three sectors under test were computed. The average results of the entire running period are given in Table 1.

The global results reported in this section, together with the results already discussed for the on line method in Section 4.1, confirm the low level of noise of the RPC system, which is well below the CMS requirements of 10 Hz/cm^2.

5. Efficiency studies

The muon trigger efficiency together with the muon reconstruction and identification efficiency are predictable once the chamber efficiencies are determined with high precision.

Efficiencies are measured in a small local region using the DT track segment extrapolation, already discussed in Section 3, with the additional requirement that in the DT chambers one and only one segment is reconstructed to reject multi-muon events like the one in Fig. 10 or other effects preventing an unambiguous prediction. Event by event, the chamber is considered efficient if a strip is fired exactly in the same η-partition where the hit was predicted, and in a fiducial region defined by ± 2 strips around the predicted strip. In Fig. 11 the local efficiency for one chamber of sector 10 of W_{+2} is reported for different values of the effective operating voltage.

The global efficiency is then evaluated as the average of the local strip by strip efficiencies. The efficiency plateau curves for four representative chambers are shown in Fig. 12.

Possible systematic uncertainties in this analysis, coming from the hit association criteria used for the analysis, are studied. In Fig. 13 the efficiency at $HV_{eff} = 9.6$ kV is given as a function of the dimension of the fiducial acceptance region expressed in number of strips. Values are normalized to the efficiency obtained for a ± 5 strip window. The figure shows that a fiducial region of ± 2 strips does not introduce any significant bias within the statistics used.

The plateau efficiencies are given in Fig. 14, where each bin corresponds to a given η-partition. In addition, the number of masked strips in the same η-partition is superimposed. The lower

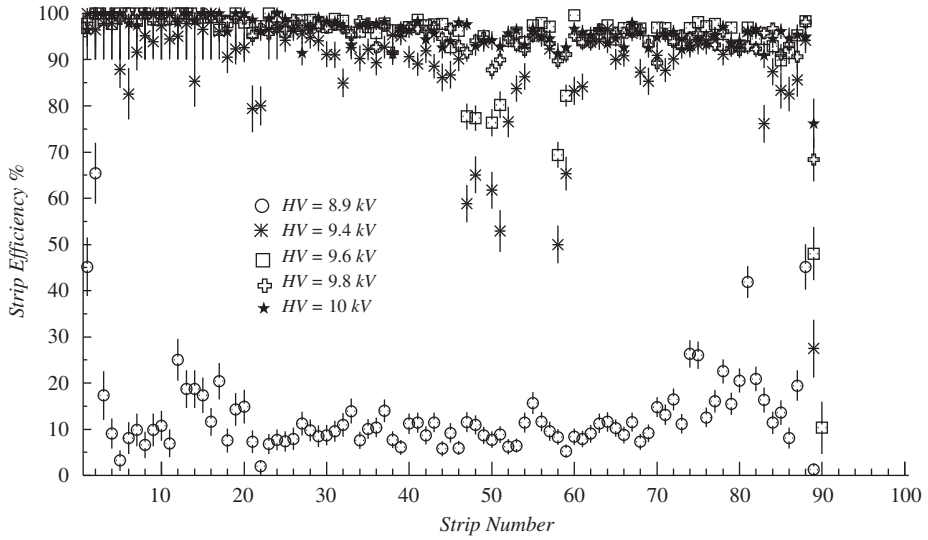

Fig. 11. Local efficiency computed along each strip for one chamber of sector 10 of W_{+2} for different values of the effective HV_{eff}.

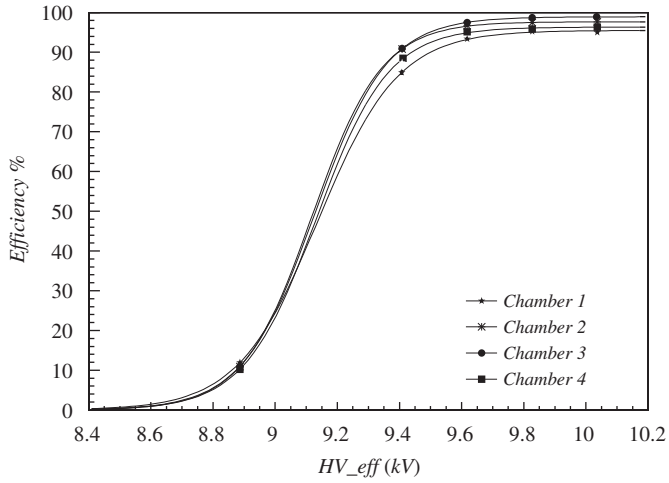

Fig. 12. Efficiency plateau for some representative chambers.

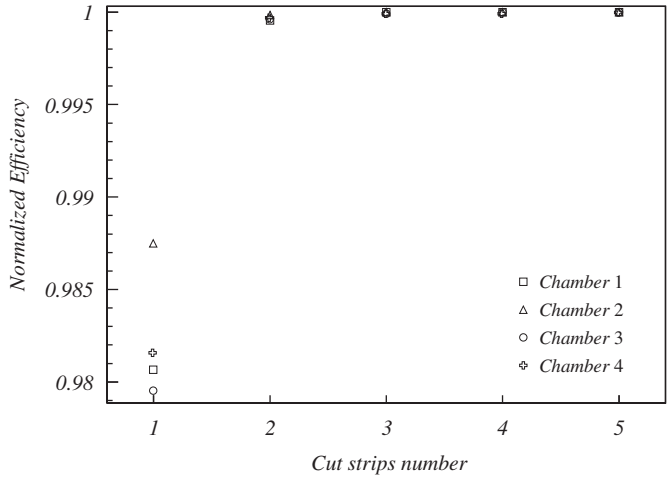

Fig. 13. Efficiency as a function of the hit acceptance fiducial region. Values are normalized to the efficiency obtained with a ± 5 strips acceptance region.

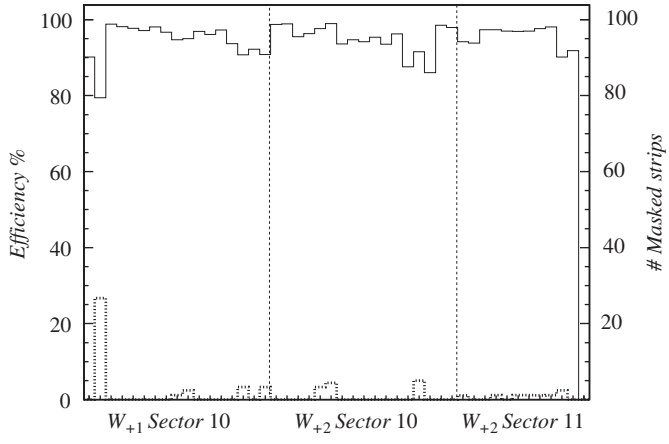

Fig. 14. Distribution of the plateau efficiencies for all the chambers in operation. Superimposed (dotted line) is the number of masked strip per chamber.

efficiency for few cases is consistent with the presence of masked strips.

Fig. 15 shows the distribution of the effective HV_{eff} for each different η-partition when chambers are operated at lower gain

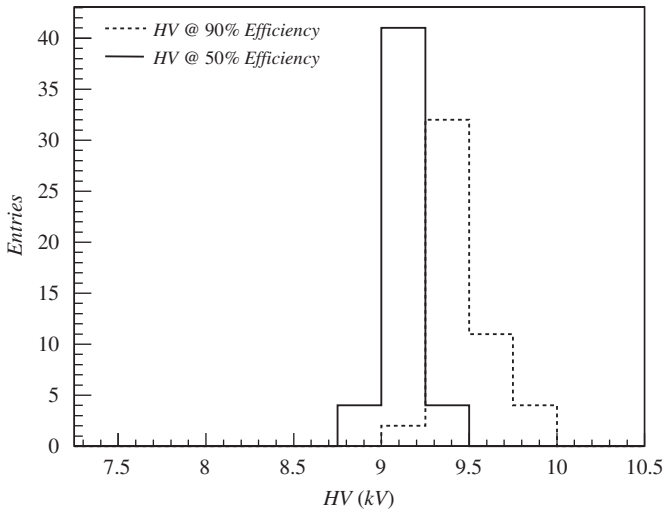

Fig. 15. Effective HV_{eff} distribution at 50%, full line, and 90%, dashed line, of the maximum efficiency.

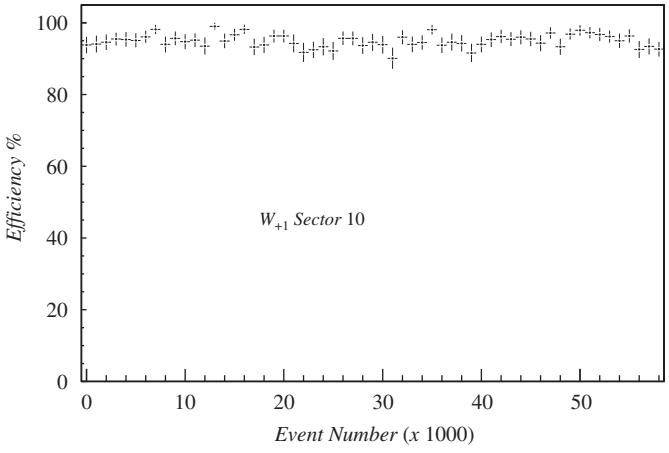

Fig. 16. Average efficiency of sector 10 in W_{+1} computed every thousand event in a typical run. Each data point corresponds to about 30 s of data taking.

when the efficiency is 50% and 90% of the maximum efficiency. The small spread denotes a good homogeneity of the RPC behavior.

Fig. 16 shows the average efficiency for sector 10 of W_{+1} computed every thousand events, to demonstrate the stability of the detector during a run.

6. Cluster size studies

The RPC trigger performance depends strongly on the hit cluster size, defined as the number of adjacent fired strips. A large cluster size could introduce uncertainty in the muon pattern recognition algorithm and originate a significant number of ghost events. The cluster size distributions at effective high voltages around the average working point are presented in Fig. 17. The increase of the average cluster size would limit the operation of the RPC system to an effective HV_{eff} value not much greater than 9.8 kV. The tail of the distributions is rather small and the maximum cluster size found was 21.

The cluster size is also studied as a function of the track impact position. The strip corresponding to the extrapolated DT segment is divided into five slices. The average cluster size is then computed for all events for each particular slice. The result is

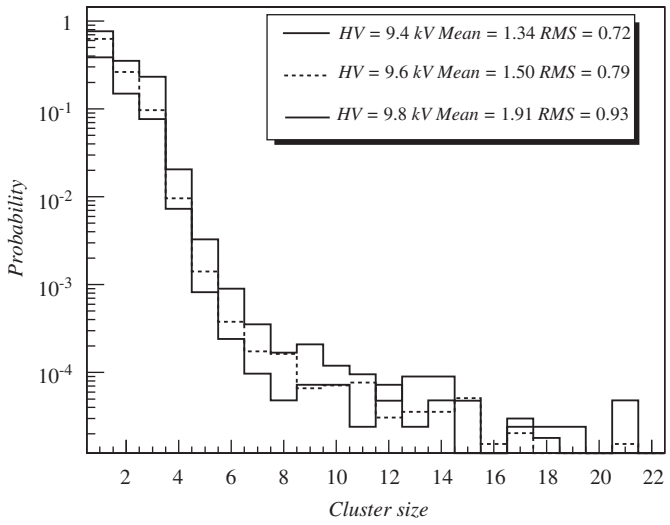

Fig. 17. Normalized cluster size distributions at different effective HV_{eff}.

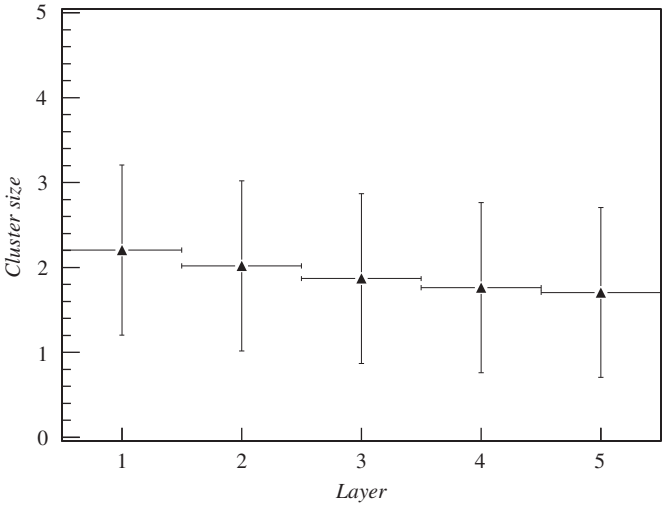

Fig. 20. Average cluster size as a function of the RPC layer.

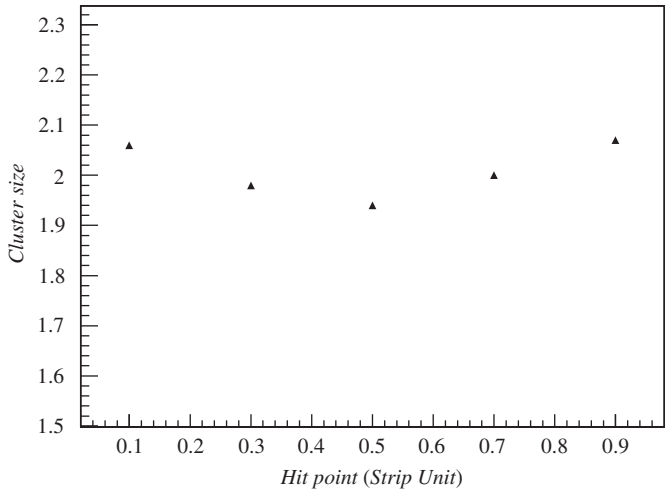

Fig. 18. Average cluster size versus the impact point on the strip. The center of the slide is considered as reference.

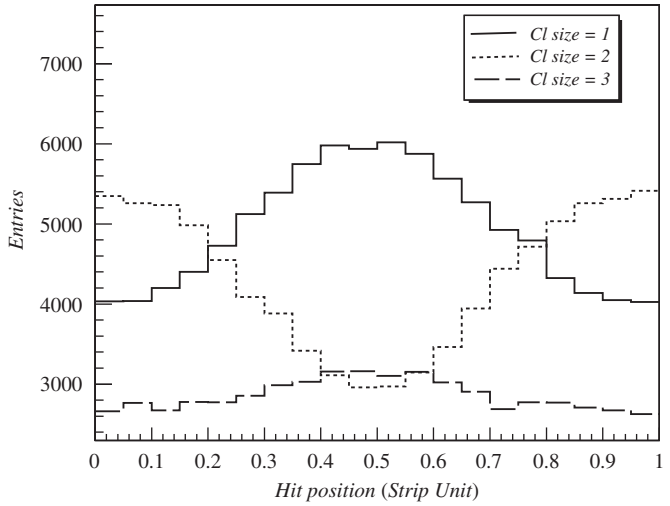

Fig. 19. Impact point distribution in strip unit for clusters of different size.

reported in Fig. 18. Average cluster size is minimal for track crossing the center of the strip, while it increases if muon hits the edges. This is confirmed by results reported in Fig. 19, where the expected impact point distributions for clusters of different sizes are shown. The strip width has also an impact on the cluster size. In Fig. 20 the average cluster size as function of the layer is given. A slight increase can be noted from outer to inner stations due to the varying width of the strips.

7. Conclusion

About 5% of the Barrel RPC Trigger system was operated in a CMS data taking period of cosmic measurements. The system behaved steadily with excellent performance with and without magnetic field. The average noise was well below $1\,Hz/cm^2$. All chambers have shown a sible-hit efficiency greater than 90%. The average cluster size per layer was below 2. All measurements are in good agreement with the previous results obtained under cosmic ray fluxes [6,13].

Acknowledgment

We would like to thank all RPC CMS technical and engineering collaborators whose valuable contribution made all this happen. This results are based on the dedicated work of the DT, DAQ, Trigger and CMS Magnet groups to whom we would like to express our gratitude. A special thank goes to the Run Coordinators, the MTCC team and our colleagues of the other sub-detector groups for their contribution to the successful operation of the test and the very collaborative atmosphere. This work was partially supported by ALFA-EC funds in the framework of the HELEN Program.

References

[1] CMS Collaboration, Technical Proposal, CERN/LHCC 94-38, 1994.
[2] CMS Collaboration, CMS MUON Technical Design Report, CERN/LHCC 97-32, 1997.
[3] CMS Collaboration, The Level-1 Trigger TDR, CERN/LHCC 2000-038, 2000.
[4] CMS Collaboration, CMS Note, The CMS Magnet Test and Cosmic Challenge (MTCC Phase I and II) Operational Experience and Lessons Learnt, 2007/05, 2007.
[5] CMS Collaboration, J. Instr. 3 (2008) S08004.

[6] M. Abbrescia, et al., Nucl. Instr. and Meth. A 359 (1995) 603.
[7] M. Abbrescia, et al., Nucl. Instr. and Meth. A 456 (2000) 143.
[8] K. Bunkowski, et al., Proc. SPIE 5125 (2003) 165–174.
[9] M. Abbrescia, et al., An RPC-based Technical Trigger for the CMS experiment, in: Proceedings of the 12 Workshop on Electronics for LHC and Future Experiments, Valentia, Spain, 25 September 2006.
[10] K. Bukowski, et al., IEEE Trans. Nucl. Sci. NS-52 (6) (2005) 3216.
[11] K. Bunkowski, et al., Meas. Sci. Technol. 18 (2007) 2446.
[12] S. Altieri, et al., Nucl. Instr. and Meth. A 461 (2001) 483.
[13] M. Abbrescia, et al., Nucl. Instr. and Meth. A 550 (2005) 116.